Available online at www.sciencedirect.com
ScienceDirect
Polymer 48 (2007) 4511–4519
polymer
www.elsevier.com/locate/polymer

Probing nucleation and growth behavior of twisted kebabs from shish scaffold in sheared polyethylene melts by in situ X-ray studies

Jong Kahk Keum, Christian Burger, Feng Zuo, Benjamin S. Hsiao*

Department of Chemistry, Stony Brook University, Stony Brook, NY 11794-3400, United States

Received 21 March 2007; received in revised form 21 May 2007; accepted 22 May 2007
Available online 26 May 2007

Abstract

By utilizing synchrotron rheo-WAXD (wide-angle X-ray diffraction) and rheo-SAXS (small-angle X-ray scattering) techniques, the nucleation and growth behavior of twisted kebabs from the shear-induced shish scaffold in entangled high-density polyethylene (HDPE) melts were investigated. The evolution of the (110) reflection intensity in WAXD at the early stages of crystallization could be described by a simplified Avrami equation, while the corresponding long period of kebabs determined by SAXS was found to decrease with time. The combined SAXS and WAXD results indicate that the kebab growth in sheared HDPE melts consists of two-dimensional geometry with thermal (sporadic) nucleation. The WAXD data clearly exhibited the transformations of (110) reflection from equatorial 2-arc to off-axis 4-arc and of (200) reflection from off-axis 4-arc to meridional 2-arc, which can be explained by the rotation of crystallographic *a*-axis around the *b*-axis during twisted kebab growth. This observation is also consistent with the orientation mode changes from 'Keller/Machin II' to 'intermediate' and then to 'Keller/Machin I'.

Keywords: Shear; Polyethylene; Shish–kebab

1. Introduction

It has been suggested that the formation of flow-induced shish–kebab structure is intimately associated with the stretch-coil transition of polymer chains in entangled melts, where the long chain species play a much more important role than the short chain species [1,2]. Due to the high entanglement in long chains, two stable conformations (i.e., stretched and coiled) can coexist in segments between the entanglement points after deformation. The stretched-chain conformation can lead to extended-chain crystallization and form shish; the shish structure can subsequently induce folded-chain crystallization of nearby coiled chain segments through an adoption process [3]. Such a mechanism is thought to form the molecular basis for flow-induced shish–kebab formation. Recently, a scanning electron microscopic (SEM) study of the extracted shish–kebab structure from ultra-high molecular weight polyethylene (UHMWPE) in a sheared polyethylene (PE) blend revealed two interesting features of flow-induced precursor structure [4]. (1) The shish structure consisted of several fibrils (so-called 'multiple-shish') instead of a single fibril typically observed in the isolated shish–kebab structure from dilute solutions [5]. (2) The kebab structure showed a single crystal-like layer structure with well defined crystallographic facets and folded-chain conformation. In this study, we aimed to deepen our understanding on the nucleation and growth behavior of twisted kebabs from the shish scaffold in the early stages of flow-induced crystallization in polyethylene (PE).

It is well known that in oriented PE samples (e.g. fibers and blown films), kebabs with folded-chain conformation are nucleated from the shish and they subsequently grow into twisted lamellae at the late stages of crystallization [2,6–10]. The lamellar twisting also takes place during spherulite growth

* Corresponding author. Tel.: +1 631 632 7793; fax: +1 631 632 6518.
E-mail address: bhsiao@notes.cc.sunysb.edu (B.S. Hsiao).

0032-3861/$ - see front matter © 2007 Elsevier Ltd. All rights reserved.
doi:10.1016/j.polymer.2007.05.057

from quiescent melts [12–17]. The schematic diagram of a twisted kebab is illustrated in Fig. 1, where the twisting process leads to rotations of crystallographic *a*-axis and *c*-axis around the *b*-axis in real space, based on an orthorhombic unit cell [6–8]. This phenomenon has been well documented by Keller et al. [2,6], Nagasawa et al. [7,8] and Schultz and Nadkarni [10]. In their studies, two scenarios of crystal orientation were presented, depending on the level of the applied stress in flow. Generally, weak flow produces kebabs in the form of twisted ribbons, resulting in off-axis (110) and meridional (200) reflections. This structure is termed as the 'Keller/Machin I' mode (or 'row orientation'). Earlier, Lindenmeyer and Lustig also observed a similar structure in tubular film using the pole figure technique; where they termed this orientation as the *a*-axis orientation [18]. In contrast, strong flow often produces kebabs in the 'Keller/Machin II' mode (or the '*c*-axis orientation'), in which the kebabs are flat and the corresponding *c*-axis remains parallel to the flow direction. The characteristic feature of this orientation is the appearance of equatorial (110) and (200) reflections. The Keller/Machin II mode has frequently been observed in HDPE blown films [9]. When the magnitude of flow is in-between the two extremes, an 'intermediate' mode can be generated, resulting in off-axis (200) and (110) reflections. It is thought that since the lateral growth of kebabs is restricted by the adjacent shish–kebab entities, the concentration of shish, which is a strong function of the applied flow, governs the degree of kebab twisting and thus the final orientation mode.

The phenomenon of lamellar twisting in PE crystals has been extensively investigated [11–17]. The origin of the twisting can be attributed to the surface stress resulted from different congestions of the fold surfaces, which was discussed by Lauritzen and Hoffman [11], Keith and Padden [12], and Lotz and Cheng [13]. Although the lamellar twisting has been well recognized in the filed of polymer crystallization, the in situ investigation of lamellar twisting, especially during the initial stage of the kebab growth, has never been reported. Some curiosities about the nucleation and growth process of twisted kebabs especially from the shish scaffold still remain. In this study, we aimed to obtain some new insights into the nucleation and growth behavior of twisted kebabs in sheared HDPE melts to fill this knowledge gap. Specifically, we have carried out 2D rheo-WAXD (wide-angle X-ray diffraction) and rheo-SAXS (small-angle X-ray scattering) measurements after cessation of a step shear. The results were analyzed by a simple shish–kebab model, consisting of central shish and sectorial twisted kebabs, in which each kebab forms sector-like fold surface as it grows outwards and gradually twists (Fig. 1). In this simple model, when the degree of lamellar twisting is very small, the changes of (110) and (200) reflection patterns are significantly affected by the outer parts of each twisting kebab. This is because the volume of individual kebab would increase as it grow outwards, where the diffraction intensity (I) is proportional to the total crystal volume (V), $I \propto V$ [19,20]. In addition, a simplified Avrami equation was applied to examine the nucleation and growth mechanism of the twisted kebabs from the shish scaffold.

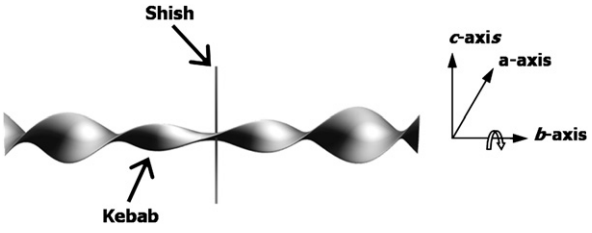

Fig. 1. A simple shish–kebab model with a single shish (shown as a thin rod) and a sectorial twisted kebab, in which the lamella extends outwards like narrow ribbon and branches into a multitude during sectorial space filling. The crystallographic axis of the kebab is indicated as illustrated.

2. Experimental

The chosen experimental HDPE sample was prepared by the Ziegler–Natta polymerization method. Its number average molecular weight, $\overline{M}_n$, and weight average molecular weight, $\overline{M}_w$, were 18,000 and 57,000 g/mol, respectively. The molecular weight distribution, MWD, of the sample was about 3.2. The sample density at ambient temperature was 0.95 g/cm^3. Synchrotron rheo-WAXD and rheo-SAXS measurements were carried out at the X27C beamline in the National Synchrotron Light Source (NSLS), Brookhaven National Laboratory (BNL). The chosen X-ray wavelength was 1.371 Å. 2D SAXS and WAXD patterns were collected with a MAR CCD detector (MARUSA) having the resolution of 1024 × 1024 pixels (pixel size = 158.44 μm). The image collection and storage times were 10 and 5 s, respectively. The sample to detector distances for SAXS (1975.6 mm) and WAXD (102.3 mm) were calibrated by AgBe (silver behenate) and Al_2O_3 (aluminum oxide) as the standards. The corrections for background scattering, air scattering, sample absorption and synchrotron beam fluctuation were carried out by using an ion chamber and a pinhole photodiode before and after the sample, respectively.

A modified Linkam shear stage with parallel plates was utilized to perform in situ X-ray measurements. The sample was subjected to a step shear at 134 °C (near the nominal melting temperature of the HDPE sample) to investigate the earliest event of the shish–kebab formation. Subsequently, the temperature was cooled down to 129 °C (at a rate of 1 °C/min) to examine the subsequent kebab growth. The chosen shear rates were 70 and 20 s^{-1}, and the shear duration time was 12 s. HDPE films with about 0.5 mm thickness were prepared by compression molding at 165 °C. Samples in the form of a ring (inner and outer diameters were 10 and 20 mm, respectively) were cut from the molded films for rheo-SAXS or rheo-WAXD measurements. A diamond disc and a Kapton film were used as X-ray windows allowing the passage of X-ray beam. The sample was placed in the gap between the two X-ray windows. Shear flow was applied to the sample by rotating the bottom window, while the top window was maintained stationary. The detailed experimental information has been described before [21].

3. Results and discussion

3.1. Comparisons of rheo-SAXS and rheo-WAXD results

Fig. 2 shows selected 2D SAXS patterns of the molten HDPE sample at 134 °C after shear (rate, $\dot{\gamma} = 70\ s^{-1}$, duration, $t_s = 12$ s) at different times. These patterns clearly exhibited the emergence of equatorial streaks immediately after shear (e.g. pattern at $t = 23$ s). The feature of equatorial streak in SAXS can be considered as the sign of shish formation (or multiple-shish formation as we speculate, since single shish may not cause the appearance of equatorial streak [4]) aligned parallel to the flow axis. The meridional maxima emerged afterwards, as seen in the SAXS pattern at $t = 38$ s. These meridional scattering peaks indicate the development of layered kebabs aligned perpendicularly to the flow direction. Although the SAXS results indicated that the evolution of the kebab assembly (leading to the lamellar stack) followed the asymptotic growth behavior, they did not provide insight into the growth mechanism of twisted kebabs.

The changes of the scattered intensity from shish (i.e., from equatorial streak) and kebabs (i.e., from meridional peaks), extracted from the 2D SAXS patterns in Fig. 2, are depicted as a function of time in Fig. 3. It was seen that shish appeared immediately upon the cessation of shear. During the entire crystallization process, the shish intensity, I_{shish}, remained about constant. However, the kebab intensity, I_{kebab}, exhibited a rapid increase. Since no crystallization was observed in the quiescent state at 134 °C (data not shown), the developments of shish and kebabs were mainly resulted from the influence of flow. The flow-induced shish formation can be explained from both thermodynamical and kinetic viewpoints. Thermodynamically, as stretched (extended) chains lead to reduced entropy, the corresponding free energy barrier for nucleation becomes less to overcome, thus easing the process of shish formation. Kinetically, since the extended-chain conformation is close to the chain conformation in the crystalline state, stretched chains encounter a less kinetics barrier to crystallize than that of the coiled state. As a result, extended-chain conformation would increase the rate of shish formation. The existence of stable shish can enable the nucleation and growth of kebabs through processes of chain diffusion and adsorption [22].

Selected 2D WAXD patterns collected during crystallization at 134 °C in the sheared HDPE melt ($\dot{\gamma} = 70\ s^{-1}$, $t_s = 12$ s) and corresponding azimuthal profiles at the (110) reflection position are shown in Fig. 4(a) and (b), respectively. The (110) azimuthal profiles were obtained using the following procedures, assuming that the sheared sample had a fiber symmetry [23]. To properly consider the (110) reflection in undistorted reciprocal space along the scattering vector

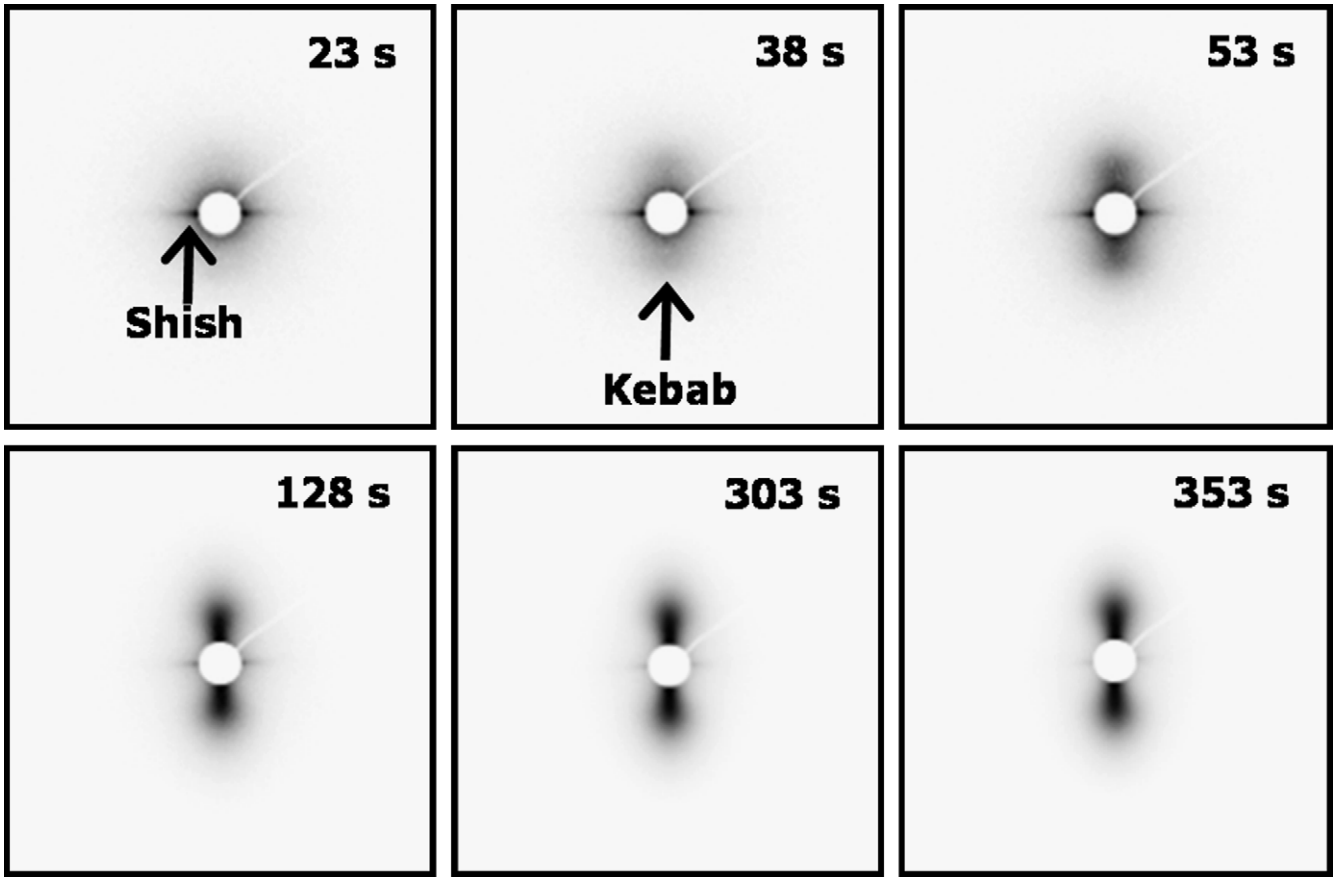

Fig. 2. Selected 2D SAXS patterns collected at 134 °C after shear (shear rate, $\dot{\gamma} = 70\ s^{-1}$, shear duration time, $t_s = 12$ s). The flow axis is vertical (we note that the shish intensity remained about constant, where the artificial decrease is due to the contrast adjustment).

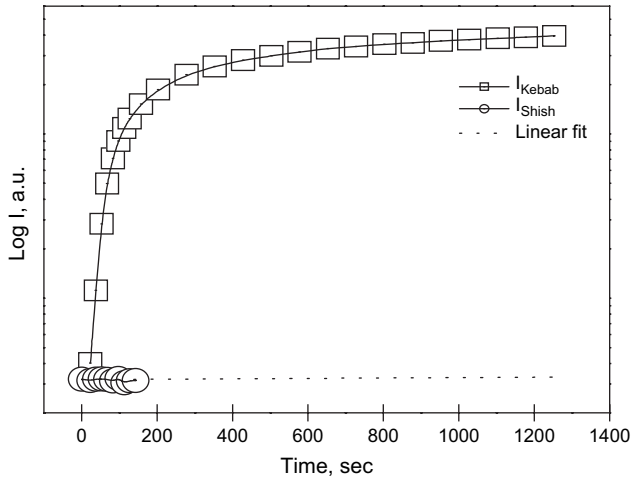

Fig. 3. The changes of scattered intensities from shish (extended-chain crystals) and kebabs (folded-chain crystals). The scattered intensity was obtained from results in Fig. 2.

($s = 2 \sin\theta/\lambda$, where θ is the half of diffraction angle and λ is the beam wavelength) and the azimuthal angle (ϕ), the measured intensity from the flat-plate detector, I (s,ϕ), was first corrected by a geometric factor, $s \cdot \sin\phi$ (we note that the 2D WAXD images in Fig. 4(a) were not corrected, but the azimuthal profiles in Fig. 4(b) were corrected; the flow axis was defined as the reference axis). In Fig. 4(a), the initial diffraction profile (e.g. $t = 98$ s) exhibited a pair of faint but highly oriented line-like (110) reflections on the equator, implying that both a-axis and b-axis were normal to the flow direction. Such a pattern is consistent with the formation of crystalline shish, having c-axis parallel to flow axis. As crystallization proceeded, the equatorial 2-arc (110) reflections were broadened azimuthally (e.g. $t = 128$ s) and then transformed into off-axis 4-arc pattern (e.g. thin arrows at $t = 263$ s in Fig. 4(a)), together with the appearance of off-axis 4-arc (200) reflections. Here, it should be noted that the amount of shish might be overestimated because the equatorial (110) intensity could also contain a fraction of kebabs formed at the early stages.

The transformation of the (110) reflection can be better examined in Fig. 4(b). In this figure, the total integrated intensity of (110) reflection was determined as $2\pi \int_{\min}^{\max} s \cdot \mathrm{d}s \int_0^{\pi/2} \sin\phi \, \mathrm{d}\phi I(s,\phi)$, where min and max represent the positions of the lowest and highest ends of the (110) crystalline peak. It was seen that the (110) reflection appeared on the equator ($\phi \approx 90°$, marked by a vertical arrow) at early stages ($t < 98$ s), but this reflection began to broaden azimuthally with increasing time (e.g. at $t = 128$ s) and eventually split into two peaks ($\phi \approx 70°$ and 110°, marked by two tilted arrows) at late stages ($t > 263$ s). The vertical arrow mark at $\phi \approx 90°$ represents the development of the shish; the tilted arrow mark pointing the (110) reflection splitting indicates the twisting of kebabs (e.g. at $t = 263$ s). The initial azimuthal broadening at the equator and then the off-axis splitting of the (110) reflection clearly revealed the evolution of kebab twisting. It is clear that as kebabs grow outwards and become twisted, the a-axis rotates around the b-axis in real space, resulting in the rotation of reciprocal vector for the (110) plane, $\bar{r}^*_{110}$. Thus, it is thought that the initial broadening of the equatorial (110) reflection can be associated with the Keller/Machin II mode, where the off-axis appearance of (110) and (200) reflections is due to the incomplete twisting of kebabs (i.e., the intermediate mode).

Using Gaussian functions, the azimuthal intensity profile of the (110) reflection in Fig. 4(b) could be curve-fitted to estimate the crystallization contributions from shish (peak at $\phi \approx 90°$) and kebabs (peaks at $\phi \approx 70°$ and 110°). The results are illustrated in Fig. 4(c). In this figure, the intensity of the equatorial (110) reflection (from shish) was found to increase initially, but reached a plateau value after $t = 98$ s. In contrast, the intensity of the off-axis (110) reflection (from twisted kebabs) increased almost linearly with time, indicating the continuous development of crystallinity.

After shear-induced crystallization at 134 °C for 45 min, further kebab growth was induced by cooling of the sample from 134 °C to 129 °C at 1 °C/min rate. The resulting degrees of crystallinity at 134–129 °C were about 2% and 10%. Selected 2D WAXD patterns collected during cooling is shown in Fig. 5. It was seen that the displacement angle of the off-axis (200) reflection gradually increased with decreasing temperature and the corresponding 4-arc pattern was transformed into a broad 2-arc pattern with (200) reflections aligned on the meridian. The observed phenomena imply change of orientation from the intermediate mode to the Keller/Machin I mode due to the further twisting of kebabs. Since the crystallinity was very low (2%) at 134 °C the shish–kebab entities were somewhat isolated without notable intra-shish–kebab impingement, where further kebab twisting was permitted.

Fig. 6 shows selected time-resolved 2D WAXD patterns of the sheared HDPE melt collected at 129 °C. In this experiment, the sample was initially sheared at 134 °C ($\dot{\gamma} = 20$ s^{-1}, $t_s = 12$ s) and then subsequently held for 45 min. Afterwards, the temperature was cooled to 129 °C at 1 °C/min. Different from the previous results at a higher shear rate ($\dot{\gamma} = 70$ s^{-1}, $t_s = 12$ s), no apparent crystallization in WAXD was observed during cooling. In addition, no equatorial streak in corresponding SAXS was seen (data not shown). However, when the temperature decreased to 129 °C, the WAXD patterns clearly developed distinct off-axis 4-arc (110) reflections at $t = 15$ s and then off-axis 4-arc (200) reflections at $t = 30$ s. This observation indicates the 2D growth of twisted kebabs, similar to that after the application of shear at a shear higher rate (70 s^{-1}). The above results are consistent with Keller's hypothesis of critical orientation molecular weight, M^* [24] as well as our results in an earlier study [21]. In brief, in a sheared polymer melt with polydispersity at a given temperature, only the chains longer than M^* can remain stretched and oriented after deformation, while the shorter chains would quickly relax back and return to the random coil state. The increase in the shear rate would decrease the value of M^* and increase the fraction of stretched chains. This hypothesis agrees well with the results after 70 s^{-1} shear at 134 °C, where a pair of equatorial line-like (110) reflections in WAXD and an equatorial scattering streak in SAXS were seen. The appearances of equatorial (110) reflections in WAXD and equatorial streak in SAXS

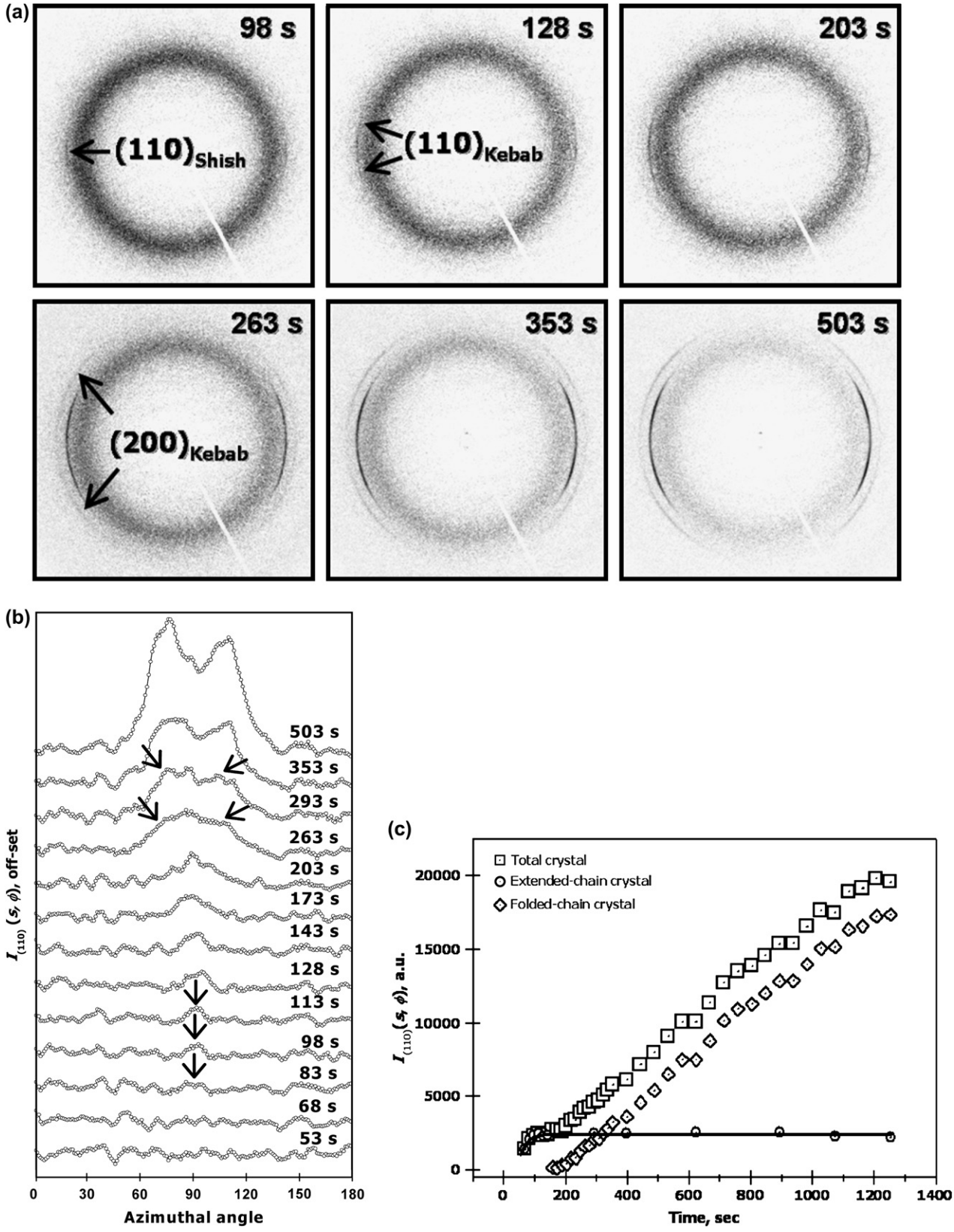

Fig. 4. (a) Selected 2D WAXD patterns collected upon crystallization at 134 °C after shear ($\dot{\gamma} = 70\ s^{-1}$, $t_s = 12$ s). (b) Corrected azimuthal intensity distributions, $I(s,\phi)$ of the (110) reflection at various crystallization times. (c) The change of diffraction intensity for the (110) plane due to flow-induced formation of shish (extended-chain crystals) and kebabs (folded-chain crystals). The (110) diffraction intensities from shish and kebabs were deconvoluted by applying Gaussian functions. The flow axis in (a) is vertical.

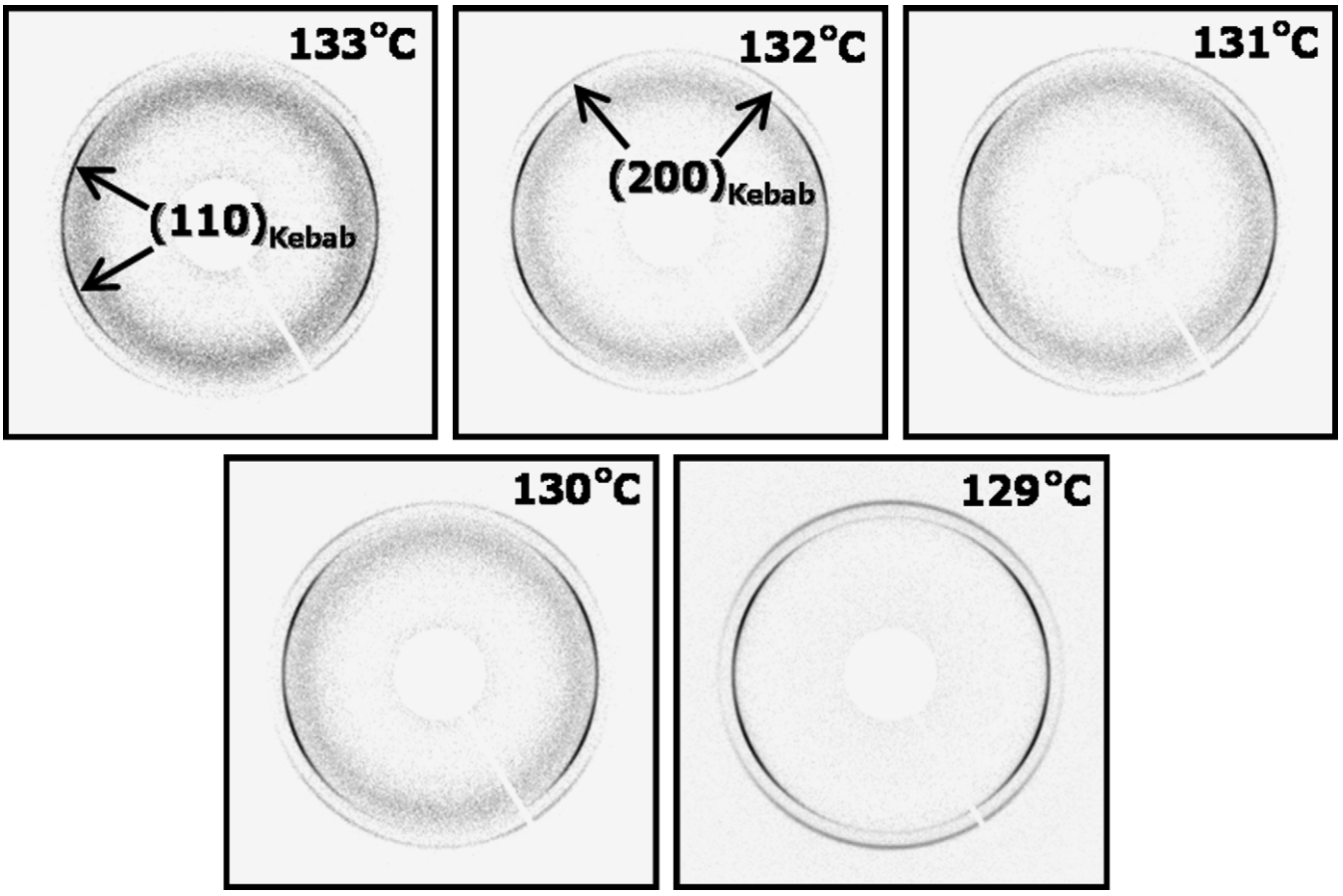

Fig. 5. 2D WAXD patterns collected during cooling (1 °C/min) from 134 °C to 129 °C. Before cooling, the melt was crystallized at 134 °C for 45 min after shear ($\dot{\gamma} = 70\ s^{-1}$, $t_s = 12$ s). The flow axis is vertical.

clearly indicate the shish formation. However, the absence of equatorial (110) reflection (Fig. 6) and equatorial scattering streak (data not shown) after the application of a lower shear rate (20 s^{-1}) at 134 °C does not necessarily indicate the absence of shish; instead it may suggest that the flow-induced shish scaffold is too weak or too dilute to be detected X-rays. Without question, this weak shish scaffold is still effective to induce kebabs at lower temperatures, as evidenced by the appearance of arc-like off-axis (110) and (200) reflections at 129 °C. Since the shish density is smaller at lower shear rates, the twisting of kebabs would be more prominent, which is consistent with the above finding.

It is noted that the transformations of (110) reflection from equatorial to off-axis and of (200) reflection from off-axis to meridian can be explained by the volume change of the individual twisting kebab (V_i), which is a function of the distance from the nucleating center (d). If one considers that the individual kebab at the initial stages prior to any physical limit can be simplified by a narrow ribbon (lamella), and the twisted kebab can branch into a multitude and fill the sectorial space, the relationship $V_i(d) \propto d^2$ should hold. However, if the physical limit is imposed (e.g. due to the concentration gradient effect), the dimension of the lamella would decrease by forming rounded growth fronts and the above relationship would not be valid. Hence, a question can be raised if the occurrence of twisted ribbon and its random branching are the only choices for the space filling process before the physical limit is reached. We believe this is the case and the following scenario is likely to occur. Based on ample microscopic evidences, one can consider that the individual kebab at the initial stages is sectorized. For example, in hexagonal shape PE single crystal, its lateral growth often exhibited sectorial habits [25]; the solvent extracted melt-crystallized shish–kebabs [4] and solution grown shish–kebabs [2] also showed the circular (or hexagonal) shape kebab morphology. The sectorial kebab can be readily twisted and then branch into a multitude and fill the space. In this scenario, the relationship, $V_i(d) \propto d^2$, can be justified.

3.2. The growth behavior of twisted kebabs in entangled melts

In order to investigate the nucleation and growth behavior of twisted kebabs, a simplified Avrami analysis was used to analyze the above results. The conventional Avrami equation can be expressed as [26]

$$v_c(t) = 1 - \exp(-Kt^n) \tag{1}$$

where $v_c(t)$ is the volume fraction of crystals at different times (t), n is the Avrami exponent and K is the Avrami constant. In semi-crystalline polymers, since the volume fraction of

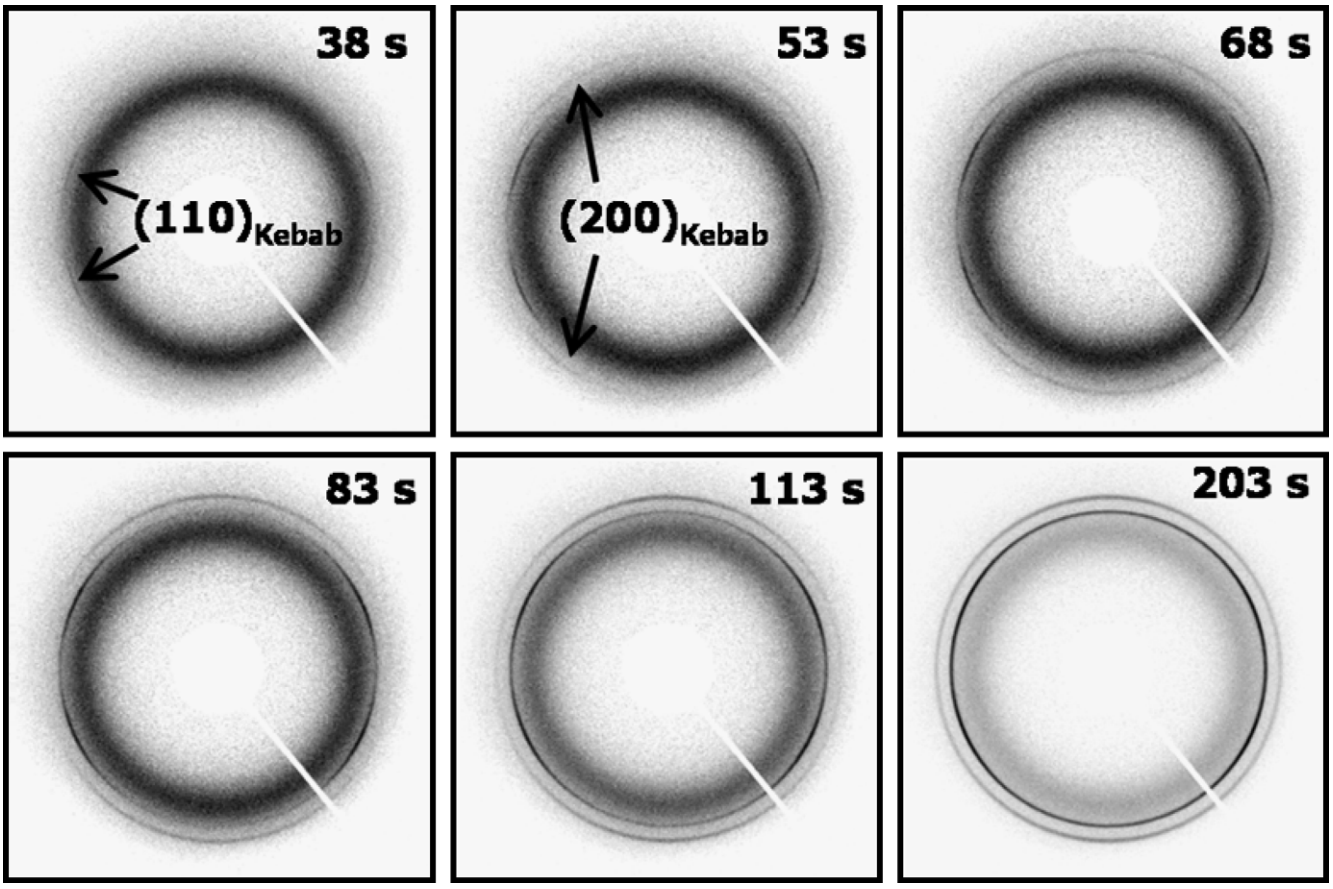

Fig. 6. Selected time-resolved 2D WAXD patterns of the sheared HDPE melt collected at 129 °C. Initially, the sample was sheared ($\dot{\gamma} = 20\ s^{-1}$, $t_s = 12$ s) at 134 °C and isothermally held for 45 min (the flow axis is vertical). The samples were subsequently cooled to 129 °C. No crystallization feature was observed at 134 °C.

crystals behind the growth front is always less than 1, the Avrami equation is often modified as [25]

$$\frac{v_c(t)}{v_\infty} = 1 - \exp(-Kt^n) \tag{2}$$

where v_∞ is the volume fraction of crystals at time infinity (∞). In the current X-ray diffraction study, the following two relationships can be assumed: (1) $v_c(t)/v_\infty$ (where $v_c(t)/v_\infty \propto$ the crystal volume $V(t)) \propto I_c(t)/I_\infty$ (where $I_c(t)/I_\infty \propto I_c(t)$), and (2) $\exp(-Kt^n) \approx 1 - Kt^n + \ldots$, where $I_c(t)$ and I_∞ are crystal reflection intensities at time (t), and infinity (∞), respectively. The Avrami equation thus becomes

$$I_c(t) \propto Kt^n \tag{3}$$

This equation indicates that during crystallization, the change in the crystal diffraction intensity as a function of time should follow a power law with an Avrami exponent (n) at the early stages of crystallization, when t is small. Such an expression should be valid at the initial stage of crystallization, but would fail at the later stage due to some physical limits such as impingements and loss of crystallizable chains.

Fig. 7 shows the relationship between the logarithmic integrated (110) intensity for only kebabs as a function of logarithmic time as well as the Avrami fits using Eq. (3) at the early stages of crystallization under two different crystallization conditions (i.e., crystallization at 134 °C immediately after shear ($\dot{\gamma} = 70\ s^{-1}$, $t_s = 12$ s) and at 129 °C after cooling from 134 °C (the sample was first sheared at 134 °C; $\dot{\gamma} = 20\ s^{-1}$, $t_s = 12$ s)). The fitted Avrami exponents' n's for both processes were found to be about 3. This suggests that the growth of twisted kebabs can either possess the 2D geometry under thermal (sporadic) nucleation or the 3D geometry under athermal (instantaneous) nucleation (Table 1). In order to determine the probable nucleation type, i.e., thermal *versus* athermal nucleation, the change in long period of the layered kebabs was also examined from the SAXS data. Under the assumption of isolated shish–kebabs structure (i.e., without the inter-shish–kebab impingement) at the initial stages, the nucleation of kebabs should be thermal if the lamellar long period decreases as a function of time; whereas the nucleation should be athermal if the long period is constant. The changes of long period for both crystallization conditions are illustrated in Fig. 8. It was found that both long periods decreased rapidly with time at the initial crystallization stage. This suggests that the nucleation process for kebabs is mainly thermal (sporadic) with 2D growth geometry, initiated from the surface of shish. It is imperative to point out that the Avrami analysis cannot distinguish the different modes of kebab growth, e.g. circular, sectorial and kebab branching.

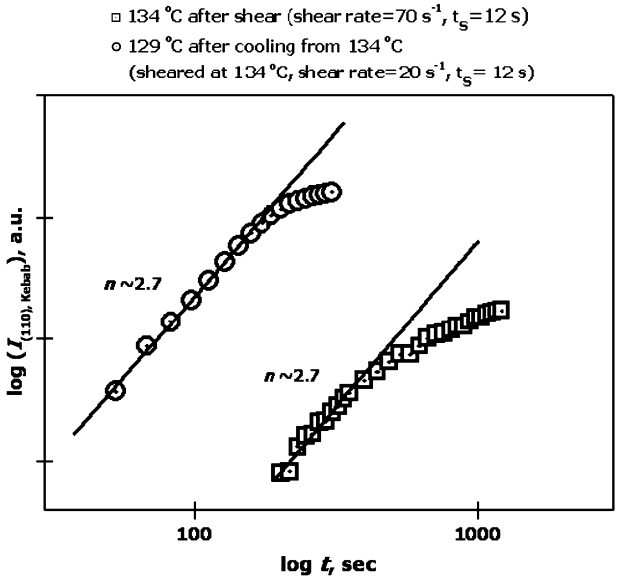

Fig. 7. The changes of the integrated (110) diffraction intensity for kebabs as a function of time (in double logarithmic scale) under two different crystallization conditions. A simplified Avrami equation (Eq. (3)) was applied at the initial crystallization stage to examine the kebab growth geometry.

Some insightful information about the growth of twisted kebabs was obtained by examining the change of displacement angle for the (110) reflection of kebabs with respect to the equator and the corresponding evolution of the (110) intensity. The results for crystallization at 134 °C after shear ($\dot{\gamma}$ = 70 s^{-1}, $t_s = 12$ s) and at 129 °C after shear at 134 °C ($\dot{\gamma}$ = 20 s^{-1}, $t_s = 12$ s) are shown in Fig. 9(a) and (b), respectively. As mentioned earlier, no crystallization was observed at 134 °C after shear at $\dot{\gamma} = 20$ s^{-1}. In Fig. 9(a), the displacement angle of (110) reflection at 134 °C was found to increase at two different rates: a sharp increase in the initial stage and a very slow increase (eventually reaching a plateau value) at $t > 600$ s. It is interesting to note that the displacement angle (twisting angle) of the (110) reflection increased only slightly at $t > 600$ s, but the corresponding increase in the (110) intensity was quite notable. This indicates that the volume of kebabs increased rather fast, even when the change in the lateral dimension of kebabs slowed down at $t > 600$ s. This would be consistent with the 2D growth of twisted kebabs, i.e., $V_i\ (d) \propto d^2$. In Fig. 9(b), the displacement angle of (110) reflection exhibited a maximum value at $t = 113$ s. The decrease in the displacement angle during twisted kebab growth indicates that the twisting angle of kebabs became higher than 90° after $t = 113$ s. This observation again confirms that a lower shish density was generated at a lower shear

Table 1
The Avrami exponent for different nucleation and growth mechanisms [24]

Growth geometry	Nucleation	
	Athermal	Thermal
Linear	1	2
Two-dimensional (2D)	2	3
Three-dimensional (3D)	3	4

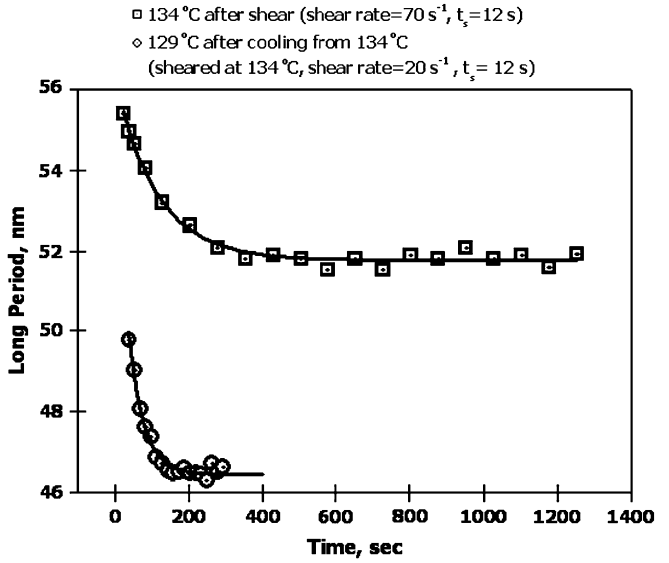

Fig. 8. The changes of long period from the SAXS data at 134 °C after shear ($\dot{\gamma} = 70$ s^{-1}, $t_s = 12$ s) and at 129 °C after cooling from 134 °C (the sample was sheared at 134 °C; $\dot{\gamma} = 20$ s^{-1}, $t_s = 12$ s).

rate ($\dot{\gamma} = 20\ s^{-1}$), in which the kebab twisting became more prominent.

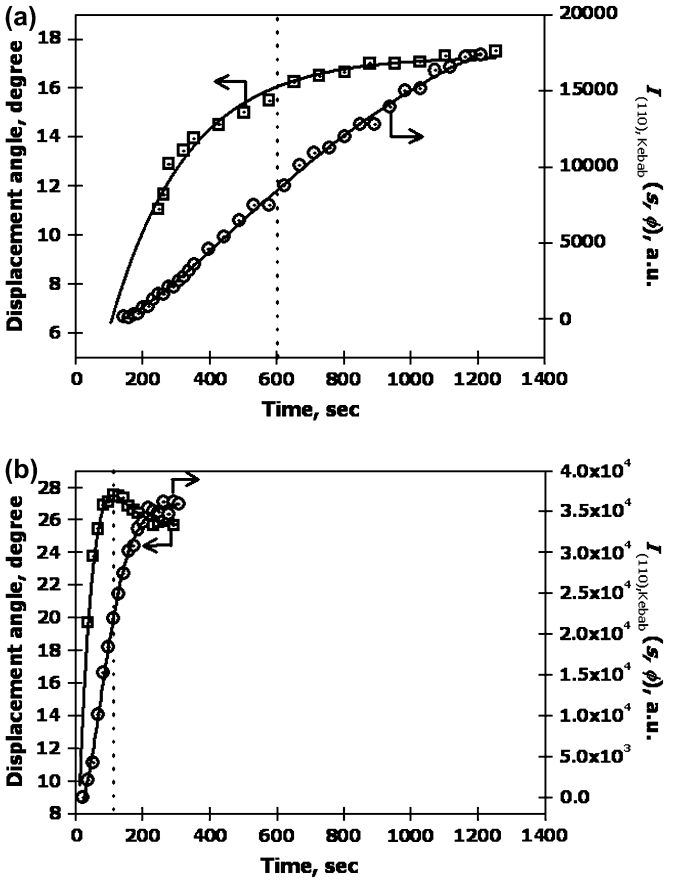

Fig. 9. The changes of the displacement angle with respect to the equator and the integrated (110) diffraction intensity during (a) crystallization at 134 °C after shear ($\dot{\gamma} = 70$ s^{-1}, $t_s = 12$ s) and (b) crystallization at 129 °C after cooling from 134 °C (the sample was sheared at 134 °C; $\dot{\gamma} = 20\ s^{-1}$, $t_s = 12$ s).

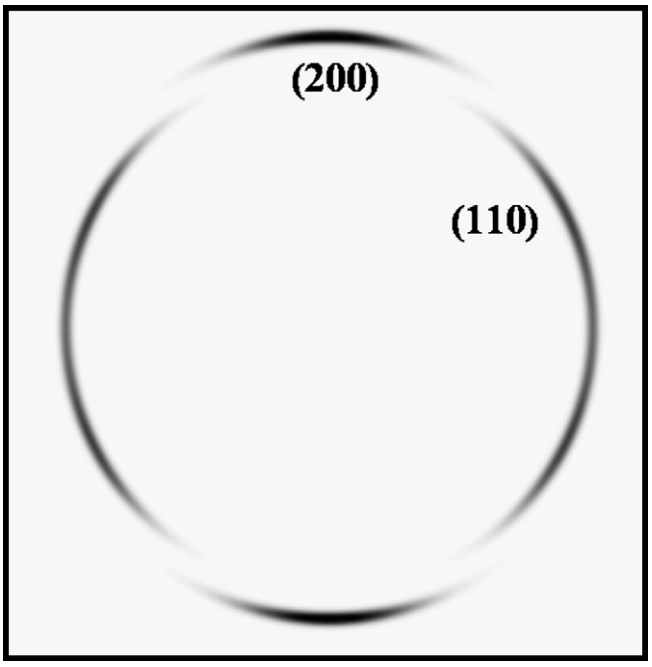

Fig. 10. Simulated 2D WAXD pattern based on the shish–kebab model in Fig. 1, where the twisting angle of the kebab was considered infinite. The flow axis is vertical.

The shish–kebab structure illustrated in Fig. 1 contains a single shish and a single twisted sectorial kebab, but this simple structure can effectively explain our X-ray diffraction results (i.e., 4-arc (110) reflections at the off-axis and 2-arc (200) reflections on the meridian). For instance, the kebab in this structure has only one rotation axis (*b*-axis) and is only moderately twisted without large extension. But this structure can be extrapolated to all directions perpendicular to the shish axis and to large extension and twisting as long as the physical limits such as the loss of crystallizable chains and the steric conflicts between the shish–kebab entities are not concerned. A calculated 2D WAXD pattern from such a simple shish–kebab model with fiber symmetry, where the twisting angle of kebabs is ''infinite'' or very large such that the orientations of *a* and *c* crystallographic axes are randomized around the *b*-axis, is shown in Fig. 10. The calculated pattern exhibits 4-arc (110) reflections at the off-axis and 2-arc (200) reflections on the meridian, which is consistent with the 'Keller/Machin I' mode proposed by Keller and Kolnaar [2].

4. Conclusions

By utilizing synchrotron rheo-WAXD and rheo-SAXS techniques, the nucleation and growth behavior of twisted kebabs from shear-induced shish scaffold in entangled HDPE melts were examined. Under strong shear (e.g. $\dot{\gamma} = 70\ s^{-1}$, $t_s = 12$ s) at 134 °C, distinct orientation changes of twisted kebabs from 'Keller/Machin II' to 'intermediate' and finally to 'Keller/Machin I' modes were seen. Under a relatively weak shear field ($\dot{\gamma} = 20\ s^{-1}$ and $t_s = 12$ s) at 134 °C, although no apparent shish was detected first, the subsequent kebab growth at 129 °C also exhibited orientation changes from 'intermediate' to 'Keller/Machin I' modes. The lower shear rate generates a lower shish density, which enhances the kebab twisting. The integrated (110) diffraction intensity of kebabs in WAXD developed at the early stages of crystallization could be described by a simplified Avrami equation, $I(s,\phi) \propto kt^n$ with $n \approx 3$, where the corresponding long period of kebabs in SAXS was found to decrease with time. The combined SAXS/WAXD results were consistent with the 2D growth of sectorial kebab under thermal (sporadic) nucleation.

Acknowledgement

We acknowledge the assistance of Drs. Igors Sics and Lixia Rong for the synchrotron SAXS and WAXD experimental setup. The financial support of this work was provided by the National Science Foundation (DMR-0405432).

References

[1] Keller A, Odell JA. Colloid Polym Sci 1985;263:181.
[2] Keller A, Kolnaar JWH. Prog Colloid Polym Sci 1993;92:81.
[3] Loos J, Katzenberg F, Petermann J. J Mater Sci 1997;32:1551.
[4] Hsiao BS, Yang L, Somani RH, Avila-Orta CA, Zhu L. Phys Rev Lett 2005;94:117802.4.
[5] Perterlin A. Pure Appl Chem 1966;12:563.
[6] Keller A, Machin MJ. J Macromol Sci Phys 1967;B1(1):41.
[7] Nagasawa T, Matsumura T, Hoshino S. Appl Polym Symp 1973;20:295.
[8] Nagasawa T, Matsumura T, Hoshino S. Appl Polym Symp 1973;20:275.
[9] Lu J, Sue HJ. Macromolecules 2001;34:2015.
[10] Nadkarni VM, Schultz JM. J Polym Sci Polym Phys Ed 1977;15:2151.
[11] Hoffman JD, Lauritzen Jr JI. J Res Natl Bur Stand (US) 1961;65A:297.
[12] Keith HD, Padden FJ. Polymer 1984;25:8.
[13] Lotz B, Cheng SZD. Polymer 2005;46:577.
[14] Bassett DC, Hodge AM. Polymer 1978;19:469.
[15] Bassett DC, Hodge AM. Proc R Soc London 1981;A377:61.
[16] Bassett DC, Hodge AM. Proc R Soc London 1979;A359:121.
[17] Schultz JM. Polymer 2003;44:433.
[18] Lindenmeyer PH, Lustig S. J Appl Polym Sci 1965;9:227.
[19] Guinier A. X-ray diffraction. San Francisco and London: W. H. Freeman and Company; 1963.
[20] Roe RJ. Methods of X-ray and neutron scattering in polymer science. New York: Oxford University Press; 2000.
[21] Somani RH, Hsiao BS, Nogales A, Srinivas S, Tsou AH, Sics I, et al. Macromolecules 2000;33:9385.
[22] Dukovski I, Muthukumar M. J Chem Phys 2003;118:6648.
[23] Fraser RDB, Macrae TP, Miller A, Rowlands RJ. J Appl Crystallogr 1976;9:81.
[24] Keller A, Kolnaar HW. Mater Sci Technol 1997;18:189.
[25] Gedde UW. Polymer physics. New York: Chapman & Hall; 1995.
[26] Avrami M. J Chem Phys 1939;7:1103.